MODELING THE CREEP BEHAVIOR OF WOOD CANTILEVER LOADED AT FREE END DURING DRYING

Mohssine Moutee
Graduate Student
Département des sciences du bois et de la forêt
Université Laval
Québec, Qc
Canada G1K 7P4

Mario Fafard
Professor
Département de génie civil
Université Laval
Québec, Qc
Canada G1K 7P4

Yves Fortin†
Professor
Département des sciences du bois et de la forêt
Université Laval
Québec, Qc
Canada G1K 7P4

and

Aziz Laghdir
Research Scientist
Département des sciences du bois et de la forêt
Université Laval
Québec, Qc
Canada G1K 7P4

(Received July 2004)

ABSTRACT

A new approach to modeling the creep behavior of a wood cantilever loaded at free end under constant moisture content and under drying conditions is developed. This approach is based on equilibrium equations of cantilever beam theory and allows the computation of stress, strain, and displacement fields through the thickness without any assumption on stress distribution. The analysis is restrained to a modified Burger model that takes into account a moisture content change in wood, although it can be extended to any type of rheological model. In constant hygrothermal conditions, the computed stress field is the same as the one based on equations of elastic cantilever. In drying conditions, a moisture gradient takes place through the thickness, and thus, a nonlinear stress distribution appears and the location of the neutral axis moves away from the geometrical center of the cross-section. The main advantage of the proposed approach is that it can be used to simulate experimental creep bending tests in the presence of moisture content gradients. Accordingly, bending tests should be appropriate to identify both viscoelastic and mechano-sorptive creep parameters.

Keywords: Cantilever, equilibrium equations, rheological model, wood drying, creep, parameter identification, bending stress, deflection.

† Member of SWST.

Wood and Fiber Science, 37(3), 2005, pp. 521 – 534

INTRODUCTION

The drying operation of wood involves three fundamental coupling mechanisms evolving with time: heat transfer, moisture content variation, and volumetric change. The development of stresses and deformations during wood drying is the consequence of these three coupling mechanisms. The complexity of the material characteristics of wood (structural heterogeneity and anisotropy, biological variability, rheological behavior, etc.) and their dependence on moisture content and temperature make difficult the elaboration of a realistic mathematical description of drying-induced stresses and deformations.

At the beginning of drying, the entire board remains in the domain of free water and only temperature-induced stresses can develop. As soon as the moisture content of the surface layers of the board drops below the fiber saturation point (FSP), the shell (the outer portion of the board) attempts to shrink. But as the core is still green, it prevents the shell from shrinking (Simpson 1991). At this moment, if a board section is removed and cut into slices parallel to the wide face, the external slices will have a shorter length than the inner ones. This displacement field is not compatible and induces, in the actual section, tensile stresses in the shell and compressive stresses in the core. When the tensile stress in the outer layers exceeds the ultimate strength of the wood, this results in surface checking.

If wood were a perfect elastic material, the stresses developed during drying would disappear as soon as moisture content and temperature profiles become uniform through the thickness of the board. However, the mechanical behavior of wood is in reality inelastic, and the shell, early in the drying process, tends toward a permanently stretched condition, called tension set. This leads to the stress reversal phenomenon, which takes place when the average moisture content of the board is near FSP (McMillen 1955; Cech 1964). The permanent stretched condition of the shell then prevents normal shrinkage of the core. This stress pattern, named case-hardening, persists until the end of drying, even after the disappearance of the moisture content and temperature gradients. A conditioning phase is normally introduced at the end of the drying process in order to relieve these residual stresses. However, conditioning does not always lead to complete stress relief, and wood distortion is then likely to occur in subsequent storage or machining. Internal checking (honeycomb) is another stress-related defect that usually occurs in the wood rays due to excessive tensile stresses in the core following stress reversal. All these stress-related drying defects can lead to important raw material and economic losses if the drying process is not properly controlled.

The study of the rheological properties of wood in situations similar to kiln-drying and the development of stress models are necessary steps toward a better understanding of the mechanical behavior of wood in drying and the control of stress-related defects. In spite of the fact that a great deal of research has been carried out in this field during the last two decades (e.g. Hisada 1986; Rice and Youngs 1990; Salin 1992; Ranta-Maunus 1992, 1993; Morén et al. 1993; Svensson 1995, 1996; Wu and Milota 1995; Perré 1996; Mårtensson and Svensson 1997; Haque et al. 2000; Ormarsson et al. 1999; Dahlblom et al. 2001; Pang 2001; Muszyński et al. 2003), more work has yet to be done to define more accurate constitutive relations between stresses and strains and to determine the viscoelastic and mechano-sorptive creep material characteristics for a wider range of species and drying conditions.

The experimental determination of the viscoelastic and mechano-sorptive creep characteristics is time-consuming and requires sophisticated procedures because of the wide range of hygrothermal conditions relevant to wood drying. Ideally, creep tests should be conducted in the three structural directions of wood and under both compression and tension loading. Mechano-sorptive tests, which are performed on specimens subjected to varying moisture conditions, must be analyzed very carefully because of the build-up of quasi-inevitable moisture gradients across the thickness of the specimens. These moisture gradients induce a nonlinear

stress pattern through the thickness, then making difficult the interpretation on the material level of the creep data obtained under such conditions. This is particularly true in the case of flexural tests because the larger dimensions of the test specimens prevent uniform moisture losses (Muszyński et al. 2003).

Most experimental works on the rheological properties of wood related to drying applications were based on tension test setups (Ranta Maunus 1975; Hisada 1986; Mårtensson 1988; Castera 1989; Hunt 1997; Hanhijärvi 1999, 2000). This allows the use of thin samples, which helps to minimize the effect of moisture gradients during mechano-sorptive tests. A few authors have conducted creep tests on both tension and compression specimens (Hisada 1979; 1980; Wu and Milota 1995). In most cases, the creep behavior of wood was found to be different for the two loading modes. As the equilibrium moisture content under load is different in tension and in compression, and because of the several factors that can affect the compression test (slenderness ratio, bulking effect, stress distribution, etc.), much care must be taken in comparing creep test results between these two loading modes. Moreover, a few studies indicated small differences in mechano-sorptive creep behavior in compression and tension (Bengtsson 1999; Svensson and Toratti 2002).

Although flexural creep tests in relation to wood drying are more prone to moisture gradient-induced stresses, they remain of great interest because of the close analogy with the mechanical behavior of wood during drying. Indeed, as mentioned above, a piece of wood at the beginning of drying has the shell in tension and the core in compression, and *vice versa* at the end of drying. Likewise, when a cantilever is subjected to a concentrated load at its free end, the upper face is in tension whereas the lower face is in compression. The experimental setup for a cantilever creep test is simple, reliable, and easily adaptable for parameter determination in the three structural directions of wood (Moutee et al. 2002). This test procedure also allows creep measurements in both tension and compression modes using bonded strain gages or optical techniques. Passard and Perré (2001) conducted bending tests under constant load on small isostress (V-shape) cantilever specimens. Deflection has been studied using elastic cantilever beam theory only, based on the hypothesis of linearity of stress distribution through the thickness of the specimen. This is obviously a very restrictive hypothesis when applying the technique in varying moisture conditions.

The objective of this study is to develop a new cantilever beam theory to model the creep behavior of wood in relation to wood drying without any assumption on the stress distribution through the thickness of the cantilever. This will allow the use of the cantilever technique for creep measurements in both constant and varying moisture content conditions. Creep modeling is based on a simple four-element rheological model (Burger model), which considers the presence of a moisture content gradient through the thickness of the cantilever. The proposed approach can be easily extended to any type of rheological model.

CANTILEVER BEAM THEORY

Problem design

This paper presents the theory of a cantilever subjected to a punctual load at free end in which the moisture content gradient effect on stress distribution is taken into account. A cantilever in its simplest form is adopted, that is a parallel-sided bar of a constant cross-section, rigidly clamped at its fixed end and loaded by a single load P at the free end acting perpendicular to the bar axis. The cantilever is analyzed using small deformation theory, which makes the problem isostatic.

The basic approach consists in modeling the mechanical behavior of the cantilever without any assumption on the stress distribution through the thickness using two equilibrium equations. These equilibrium equations should be satisfied all along the length of the cantilever. The stresses obtained from the time-dependent rheological model will be integrated over the thickness of the cantilever and used in the two

global equilibrium equations. The curvature of the cantilever will be estimated from the assumed linear strain distribution over the thickness and the neutral axis position of this profile (Euler-Bernoulli hypothesis). Knowing the curvature in function of time, the deflection of any point along the cantilever will be calculated. Thus, from laboratory test displacement measurements (surface strain or deflection) in drying or non-drying conditions, this mathematical model in conjunction with an optimization algorithm could be used to estimate the parameters of the model by minimizing the difference between the measured displacements and the computed ones.

Considering an orthotropic cantilever with dimension $l \times b \times h$ (length × width × thickness) (Fig. 1), a Cartesian coordinate system (x, y, z) is used, where x is the axial coordinate, z the thickness coordinate, and y is normal to the symmetrical xz-plane. Fixed at $x = 0$ and loaded at $x = l$, the material properties, stresses, and strains are assumed to be dependent only on the z-coordinate; and the relationship between stress and strain is assumed to be nonlinear. The externally induced strain, function of the x-coordinate, forces the cantilever to bend in xz-plane. For slender cantilevers $\left(\frac{l}{h} > 10\right)$, the influence of shear is neglected and the normal stress components σ_{yy},σ_{zz} are assumed to be negligible when compared to the axial stress σ_{xx}. Hence a uniaxial state of stress is considered.

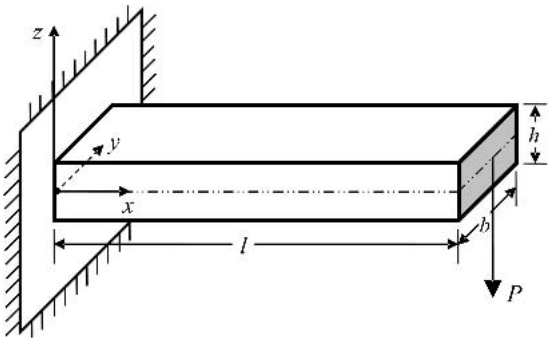

FIG. 1. Orthotropic cantilever (l = length; b = width and h = thickness) subjected to a punctual load P at free end.

The out-of-plane displacement w (deflection), which is defined as the distance between the cantilever neutral plane and its unloaded position, is accompanied by a rotation of the cantilever neutral plane, defined as θ (Fig. 2). The function $u(x, z)$ is the displacement in the x-direction across the thickness, which is linked to strain $\varepsilon(x, z)$ by the equation, $\varepsilon(x, z) = \frac{d}{dx} u(x, z)$. Using the small deformation theory, we can write $\sin \theta \approx \theta$ and

$$u(x, z) = -\theta(x) \cdot z \tag{1}$$

Derivation of deflection curve

According to the Euler-Bernoulli beam assumption, a cross-section which is plane and perpendicular to the axis of the undeformed beam remains plane and perpendicular to the deflection curve of the deformed beam (Batoz and Dhatt 1990). Using this assumption and Eq. (1), we can safely assume that there is negligible strain in the z direction ($\varepsilon_z = 0$); the strain distribution throughout the cantilever is

$$\varepsilon(x, z) = \frac{d}{dx} u(x, z) = \chi(x) \cdot z \tag{2}$$

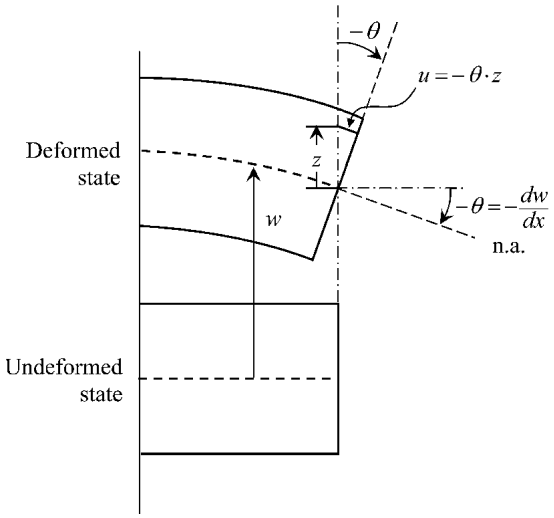

FIG. 2. Kinematic assumptions of Euler-Bernoulli.

where $\chi(x)$ represents the curvature radius of the cantilever

$$\chi(x) = -\frac{d\theta(x)}{dx} \tag{3}$$

With the assumption that a plane cross-section remains plane after deformation, we have

$$\theta(x) = \frac{dw(x)}{dx} \tag{4}$$

where $w(x)$ is the cantilever deflection. Combining Eqs. (3) and (4), we obtain

$$\chi(x) = -\frac{d^2w(x)}{dx^2} \tag{5}$$

Finally, with boundary conditions at fixed end, $w(x)|_{x=0} = 0$ and $\theta(x)|_{x=0} = \frac{d}{dx}w(x)\Big|_{x=0} = 0$, the deflection curve all along the cantilever can be calculated using the following equation:

$$w(x) = \int_0^x \int_0^x \chi(u)\, du \tag{6}$$

For elastic material, the stress-strain relationship is given by Hooke's law

$$\varepsilon(x, z) = \frac{\sigma(x, z)}{E}$$

where E is the Young's modulus. In the elastic cantilever beam theory, since the strain is assumed linear through the thickness, the stress is also linear through thickness due to Hooke's law, and the maximum tensile and compressive stresses, σ^t and σ^c at $z = \pm h/2$ are equal in absolute value

$$\sigma^t = |\sigma^c| = \frac{\mathcal{M}}{I_z} \cdot \frac{h}{2} = \frac{P(l-x)}{I_z} \cdot \frac{h}{2} \tag{7}$$

where $I_z = \frac{b \cdot h^3}{12}$, $\mathcal{M}$ is the resulting bending moment of load P, and h the thickness. Thus, from the two later equations, we obtain the relation

$$\varepsilon(z) = \frac{\sigma(z)}{E} = \frac{\mathcal{M}}{EI_z} \cdot z$$

Regarding Eq. (2), we can write

$$\chi(x) = \frac{\mathcal{M}}{EI_z}$$

and from Eq. (6), we obtain the well-known elastic deflection at free end

$$\delta_{\max} = w(x)|_{x=l} = Pl^3/3EI_z$$

The bending deflection of a cantilever is generally considered as being proportional to the applied load. This assumption of elastic behavior is sufficient for the analysis of wood structure, but this is true only for short-term observation and low load level. Even when submitted to a constant load, the cantilever deflection increases with time. This is the creep phenomenon. The magnitude of creep depends on moisture content, temperature, and load level. This will be developed later in the text.

Cantilever equilibrium equations

Figure 3 shows the strain distribution at coordinate x, using the Euler-Bernoulli assumption; the total strain distribution is linear through the thickness, and we can write

$$\varepsilon(z) = \varepsilon_{uf} \times \frac{z - z_0}{h/2 - z_0} \tag{8}$$

where ε_{uf} is the strain at $z = h/2$ and z_0 is the position of the neutral axis (*n.a.*) relative to the geometric axis where the total strain is zero. Therefore, we have two unknown variables (ε_{uf} and z_0), meaning that two equations are required to determine the two values. These equations are equilibrium equations of cantilever beam theory (Batoz and Dhatt 1990). Assuming that the neutral axis does not coincide with the geometric axis, the cantilever equilibrium equations are:

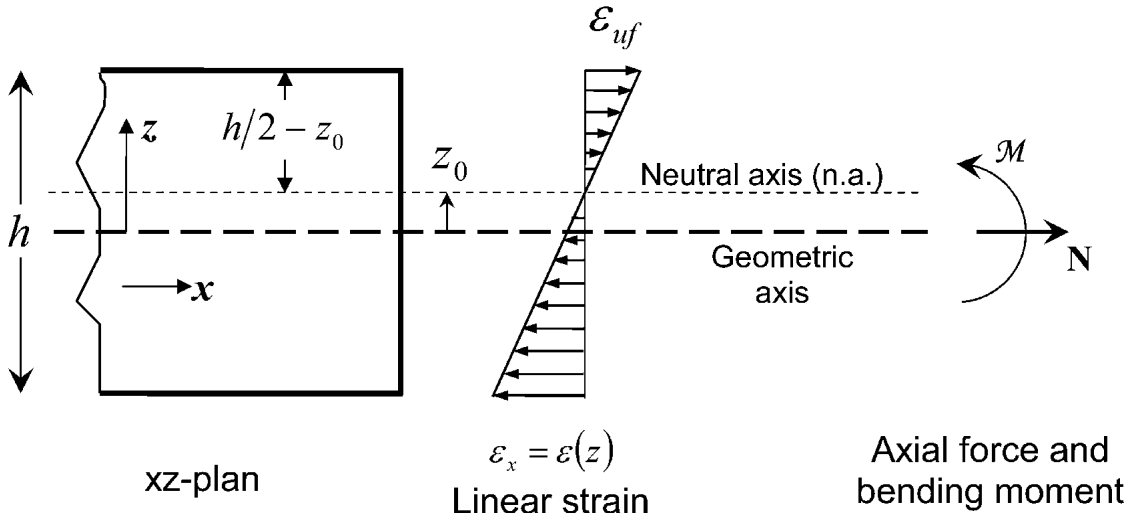

FIG. 3. Schematic of cantilever thickness (*xz*-plan) at given *x*-position, z_0 is the location of the neutral axis (*n.a.*).

$$R_{\mathcal{M}} \equiv b \cdot \int_{-h/2}^{h/2} \sigma(x, z) \cdot (z - z_0)\, dz - \mathcal{M}(x) = 0 \tag{9a}$$

$$R_N \equiv b \cdot \int_{-h/2}^{h/2} \sigma(x, z)\, dz = 0 \tag{9b}$$

where σ is the stress distribution through the thickness, z_0 is the position of the neutral axis, and $\mathcal{M} = P(l - x)$ is the resulting bending moment at coordinate x due to the applied load P. Because no axial load was assumed, the integral of all stresses through the cantilever cross-section must be equal to zero (Eq. 9b). The sign of z is positive when locating fibers above the neutral axis and negative for fibers beneath the neutral axis. The load will provide tensile stresses σ_t^+ in all fibers lying on the positive side of the neutral axis. Compressive stresses σ_c^- exist in all fibers beneath the neutral axis, where z is negative.

Up to this point, the cantilever beam theory was established without taking into account the stress-strain relation. If the stress-strain relation is established adopting rheological mathematical models, Eqs. (9) can be solved numerically and simultaneously for ε_{uf} and z_0. This is done by a simple time-stepping procedure, where iterations are made for each time step until equilibrium is obtained. This means that, when constitutive equations describing the linear or nonlinear stress-strain relation are established, the determination of stress field can be done by numerical integration of Eqs (9).

For a given time and for a given position x, the values of ε_{uf} and z_0 are computed iteratively. An integration scheme through the thickness of the cantilever is used to estimate the two equilibrium equations. Thus, these equations can be rewritten as:

$$R_{\mathcal{M}} \equiv b \cdot \sum_{n=1}^{N_{layer}} [\sigma(x, z_n) \cdot (z_n - z_0) W_n] - \mathcal{M}(x) = 0 \tag{10a}$$

$$R_N \equiv b \cdot \sum_{n=1}^{N_{layer}} \sigma(x, z_n) W_n = 0 \tag{10b}$$

where W_n is the weight relied to the integration scheme and z_n is the location of the layer at which the stress is evaluated using an appropriate rheological model.

If Eqs. (9) are satisfied along the cantilever, we know the value of ε_{uf} and z_0 at any coordinate x and at any time t. Thus, we can calculate the curvature from the following equation:

$$\chi = \frac{\varepsilon_{uf}(x, t)}{h/2 - z_0(x, t)}$$

Using Eq. (6), the deflection of the cantilever will be known at any position and at any time.

The main advantage of the above-described approach is that the proposed cantilever beam theory is completely independent of the stress-strain relation. The stress-strain relation could be linear or nonlinear and time-dependent or not. We only need to solve the constitutive model to estimate the stress at the given location in time and space (*t, x, z*). No assumption is needed on the stress distribution through the thickness. The proposed approach is therefore more general.

RHEOLOGICAL MODEL

Since the aim of this paper is not to develop a new rheological model as such, creep modeling will be restrained to a modified Burger model in which moisture content change in wood is taken into account as well as shrinkage strain (Fig. 4).

Burger model (viscoelastic creep model)

For the purpose of this study, it is assumed that the four-element Burger model is adequate to predict the creep response of wood (Senft and Suddarth 1970; Hoyle et al. 1986; Fridley et al. 1992). The Burger model will, however, be modified to account for moisture change effects. It should be noted that the Burger model is valid only for primary and secondary creep behavior, and that tertiary creep is not predicted by the model (Fridley et al. 1992).

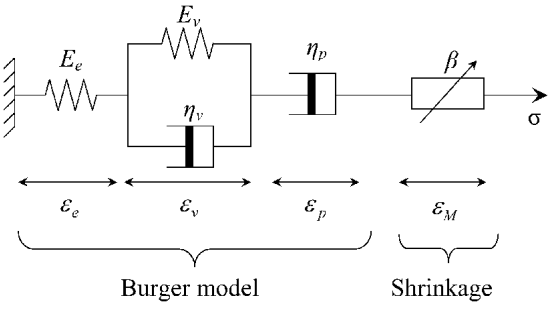

FIG. 4. Four-element rheological model (Burger model) with shrinkage component.

Constitutive equations in 1-D.—In an uniaxial Burger rheological behavior (1-D), it is assumed that the total strain $\varepsilon = \varepsilon(t,T,M)$ is composed of three components: elastic strain (ε_e), viscoelastic strain (ε_v) (completely recoverable), and "visco-plastic" strain (ε_p) (permanent deformation), in addition to the deformation due to free shrinkage (ε_M) and temperature change (ε_T). The total strain ε is written as follows:

$$\varepsilon = \varepsilon_e + \varepsilon_v + \varepsilon_p + \varepsilon_M + \varepsilon_T \tag{11}$$

The mathematical expressions for the three first components of strain (Burger) are:

$$\sigma = E_e \varepsilon_e \tag{12}$$

$$\sigma = E_v \varepsilon_v + \eta_v \dot{\varepsilon}_v \tag{13}$$

$$\sigma = \eta_p \dot{\varepsilon}_p \tag{14}$$

where σ is the applied stress, E_e the Hookean spring constant associated with elastic deformation, E_v and η_v the Hookean spring constant and viscosity of the Newtonian dashpot, respectively, of the Kelvin element, and η_p the viscosity of the Newtonian dashpot associated with unrecoverable strain. The over-dot represents the time derivative.

In constant moisture content conditions, the analytical formulation of strain-stress relationship of Burger model is (Bodig and Jane 1982):

$$\varepsilon = \frac{\sigma}{E_e} + \frac{\sigma}{E_v}\left[1 - \exp\left(-\frac{E_v}{\eta_v} \cdot t\right)\right] + \frac{\sigma}{\eta_p} \cdot t \tag{15}$$

Free shrinkage strain rate.—Shrinkage appears in all parts of the board for which the moisture content (MC) is within the hygroscopic range.

$$\dot{\varepsilon}_M = \frac{d\varepsilon_M}{dt} = \beta \frac{dM_{fsp}}{dt} \tag{16}$$

where β is the shrinkage/swelling coefficient (independent of moisture) and dM_{fsp}/dt is the drying rate below FSP.

Hygrothermal effects

Moisture content and temperature are known to affect the mechanical properties of wood. In the case of the four-elements model defined previously, the values of E_e, E_v, η_v and η_p must be adjusted for their hygrothermal state. Only the moisture effect was considered in this study. The elastic modulus depends on moisture content according to the formulation proposed by Guitard (1987):

$$E_i^M = E_i^{12}[1 - 0.015(M - 12)] \qquad (17)$$

where E_i^M is the elastic modulus at the actual MC (i=e, v); E_i^{12} is the elastic modulus at 12% MC. Equation (17) is valid for moisture content between 6% and FSP. As no information was available about moisture content effect on viscous parameters (η_v and η_p), we adopted the same relation as in Eq. (17), i.e.

$$\eta_i^M = \eta_i^{12}[1 - 0.015(M - 12)] \qquad (18)$$

NUMERICAL METHODS

The cantilever beam theory and the creep model presented in the previous sections can be combined to perform simulations of the cantilever under various loading and moisture conditions. In order to do so, the overall model has to be implemented into a computer program.

Whether the simulation used is one- or two-dimensional, there are some aspects that have to be recognized. The implemented model is nonlinear, and the description of the development of stresses and strains is history-dependent. This means that an incremental formulation must be used.

Having a given constitutive model (Burger model), we can solve the cantilever equilibrium Eqs. (10a) and (10b). Therefore, we need to reformulate Eqs. (11) to (14) into stress at x and z position of a cantilever subjected to a single load P at the free end. Equation (11), can be written as

$$\varepsilon_e = \varepsilon - \varepsilon_v - \varepsilon_p - \varepsilon_M = \sigma/E_e \Rightarrow$$
$$\sigma = E_e \cdot (\varepsilon - \varepsilon_v - \varepsilon_p - \varepsilon_M) \qquad (19)$$

Substituting (19) into Eqs. (13) and (14), we obtain

$$\begin{cases} \eta_v\dot{\varepsilon}_v + (E_e + E_v) \cdot \varepsilon_v + E_e \cdot \varepsilon_p = E_e \cdot (\varepsilon - \varepsilon_M) \\ \eta_p\dot{\varepsilon}_p + E_e\varepsilon_p + E_e\varepsilon_v = E_e \cdot (\varepsilon - \varepsilon_M) \end{cases}$$

In matrix notation we have:

$$\begin{bmatrix} \eta_v & 0 \\ 0 & \eta_p \end{bmatrix} \begin{Bmatrix} \dot{\varepsilon}_v \\ \dot{\varepsilon}_p \end{Bmatrix} + \begin{bmatrix} E_e + E_v & E_e \\ E_e & E_e \end{bmatrix} \begin{Bmatrix} \varepsilon_v \\ \varepsilon_p \end{Bmatrix} = \begin{Bmatrix} E_e \cdot (\varepsilon - \varepsilon_M) \\ E_e \cdot (\varepsilon - \varepsilon_M) \end{Bmatrix} \qquad (20)$$

We adopt the α – *scheme* for time discretization:

$$\{\varepsilon_i\}^{k+1} = \{\varepsilon_i\}^k + \Delta t[(1 - \alpha)\{\dot{\varepsilon}_i\}^k + \alpha\{\dot{\varepsilon}_i\}^{k+1}] \qquad (21)$$

where $i = v, p$ and k is the time step number. Using an implicit scheme $\alpha = 1$, Eq. (20) becomes:

$$\begin{bmatrix} \frac{\eta_v}{\Delta t} + E_e + E_v & E_e \\ E_e & \frac{\eta_p}{\Delta t} + E_e \end{bmatrix} \begin{Bmatrix} \varepsilon_v \\ \varepsilon_p \end{Bmatrix}^{k+1} = \begin{bmatrix} \frac{\eta_v}{\Delta t} & 0 \\ 0 & \frac{\eta_p}{\Delta t} \end{bmatrix} \begin{Bmatrix} \varepsilon_v \\ \varepsilon_p \end{Bmatrix}^k + \begin{Bmatrix} 1 \\ 1 \end{Bmatrix} E_e \cdot (\varepsilon - \varepsilon_M)^{k+1} \qquad (22)$$

Note that all physical parameters in Eq. (22) must be evaluated at time $k+1$ using Eqs. (17) and (18). The numerical procedure consists of solving Eqs. (10a) and (10b) for ε_{uf} and z_0. This is done by dividing the board into n layers of equal thickness, and by means of a simple time-stepping procedure, iterations are made for each time step until equilibrium is obtained. Therefore the strain field $\varepsilon(z)$ and stress field $\sigma(z)$ are simultaneously computed at (x, z) position.

For a cantilever in drying conditions, we need a one-dimensional water transport history to be used as input for drying stress simulations. Thus, a parabolic function was chosen to simulate theoretical moisture content profiles through thickness with respect to time (Fig. 5):

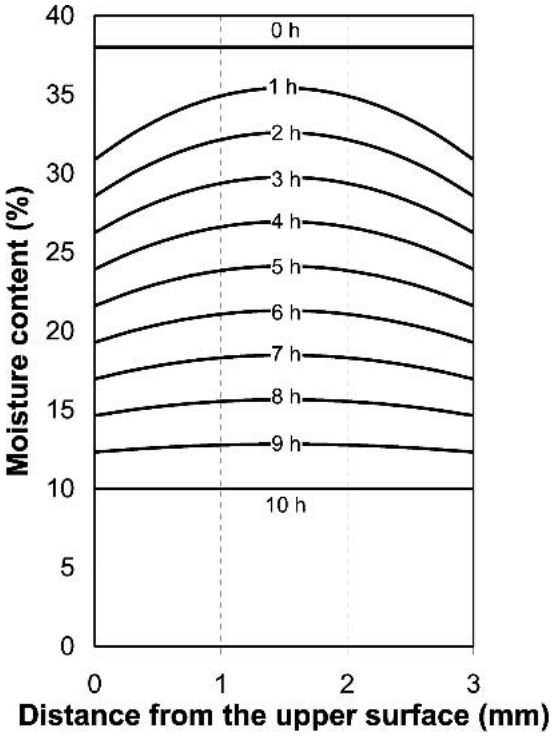

FIG. 5. Moisture content profile through thickness z for a drying of 10 h.

$$M(z, t) = a(t) \cdot z^2 + b(t) \cdot z + c(t)$$

where $a(t)$, $b(t)$, and $c(t)$ are polynomial coefficients evolving with time. The total drying time from 38% to 10% MC was assumed to be 10 h with a constant drying rate from start to finish.

The numerical procedure was developed using Maple 9 Engineering Software under Windows 32-bits platform.

RESULTS AND DISCUSSION

A longitudinal oriented specimen of dimensions $l = 100$ mm, $h = 3$ mm, $b = 25$ mm was considered for the simulations. Burger model parameters at 12% MC were taken as: $E_e =$ 10,400 MPa, $E_v =$ 10,000 MPa, $\eta_v =$ 10,000 MPa.h, and $\eta_p =$ 239,000 MPa.h. Longitudinal shrinkage was assumed to be linear with a total shrinkage coefficient $\beta = 0.3\%$. Note that except for Young's modulus, which is representative of white spruce (*Picea glauca* (Moench.) Voss.) wood at ambient temperature, the above Burger parameter values are only very rough estimates deduced from preliminary creep tests. Furthermore, the value of η_v was deliberately lowered in order to amplify for graphical representation the viscoelastic creep deformation, which is normally very small at ambient temperature. All the simulations were run at constant temperature.

Creep in constant conditions

The first analysis consists in simulating the creep in constant moisture conditions (18% MC) under the load levels of 742 g and 247 g, corresponding to 30% and 10% of bending strength (MOR) at quarter span ($x = l/4$), respectively. The loading time is 300 min. The same time period is used for the recovery part. The simulation results are shown in Figs. 6a (surface stress) and 6b (surface strain). The analytical solution of creep (Eqs. 7 and 15) for the load of 742 g is reported for comparison with the numerical simulation.

The computed stress is the same as the one using elastic cantilever beam theory equation (Eq. 7) for each given load. As expected, total surface creep increases with increasing stress level. For the load of 742 g, the surface creep and creep recovery computed from the simulation model are identical to the analytical calculations from Eq. (15), which proves the accuracy of the simulation model. As moisture content is constant, there are no drying-induced stresses; thus, the stress distribution through the thickness is linear and the neutral axis coincides with the geometrical center of the cross-section.

Figure 7 presents the computed deflection time-dependent $w(t)$ at free end ($x = l$) for a load of 742 g. The deflection curve exhibits a similar shape as the surface strain curve (Fig. 6b) since the deflection is inferred from the axial strain. One must recall that deflection in function of time can be estimated at any position along the cantilever.

Creep in drying conditions

The creep behavior of the cantilever under load is affected during drying. The moisture

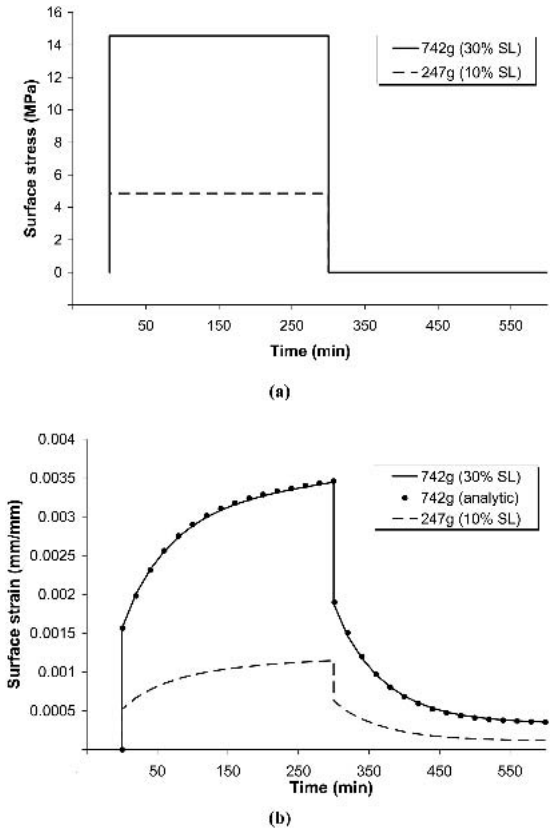

FIG. 6. Simulations of stress and tensile surface creep/recovery creep at $x = l/4$ from fixed end for two loads (742 g and 247 g) at 18% MC, unloaded after 300 min. a. Surface stress and; b. Surface strain.

content history imposed for this test was given in Fig. 5. Under such conditions, the shrinkage strain must be added to the Burger model. In order to have the same surface stress (14.57 MPa) than in constant moisture conditions (Fig. 6a), a load of 557 g was considered for the simulation, which corresponds to about 50% MOR for green white spruce wood. The drying procedure begins 5 min after load application. The simulation results obtained at quarter span are shown in Fig. 8. Figure 8a compares the computed stress vs. time for constant and varying moisture conditions. As the drying of wood induces shrinkage below FSP, drying stresses appear. Reporting the stress profile through the thickness for both conditions after 120 min of drying (Fig. 8b), we can see that in drying conditions the stress is nonlinear and the location of the neutral axis moves away from the geometric center of the cross-section. Thus, it is clear that under drying conditions, the stress field cannot be estimated from the classical elastic cantilever beam theory.

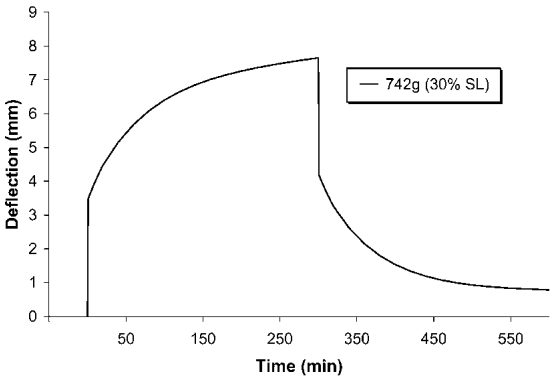

FIG. 7. Deflection at free end ($x = l$) for a load of 742 g (30% SL) and 18% MC.

Figure 9 shows for the same simulation the total strain, the shrinkage strain, and the pure creep strain at the upper face of the cantilever. The creep strain is obtained by subtracting shrinkage strain from total strain. Shrinkage strain is negative deformation, whereas creep strain at the upper face is positive due to the applied load. Thus, at the upper face, the shrinkage decreases the total strain during load application and *vice versa* after unloading.

Drying stress without load

Another simulation was run to study stress and strain evolution in the cantilever during drying but with no load applied at free end. This represents the case of purely drying-induced stresses as a result of moisture content change. The drying schedule imposed for this test was given in Fig. 5, except that in this case the initial moisture content was set at 35% so as to shorten the drying above FSP. Figure 10 shows the result of stress simulation at the surface and at the center of the board during drying. After about 30 min the moisture content at the wood surface drops below FSP. With further drying, the sur-

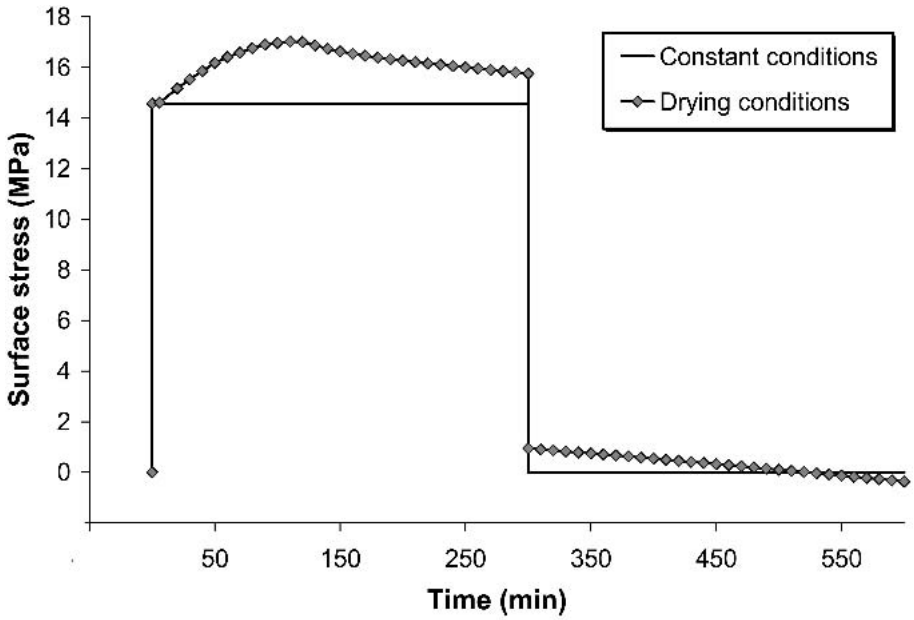

(a)

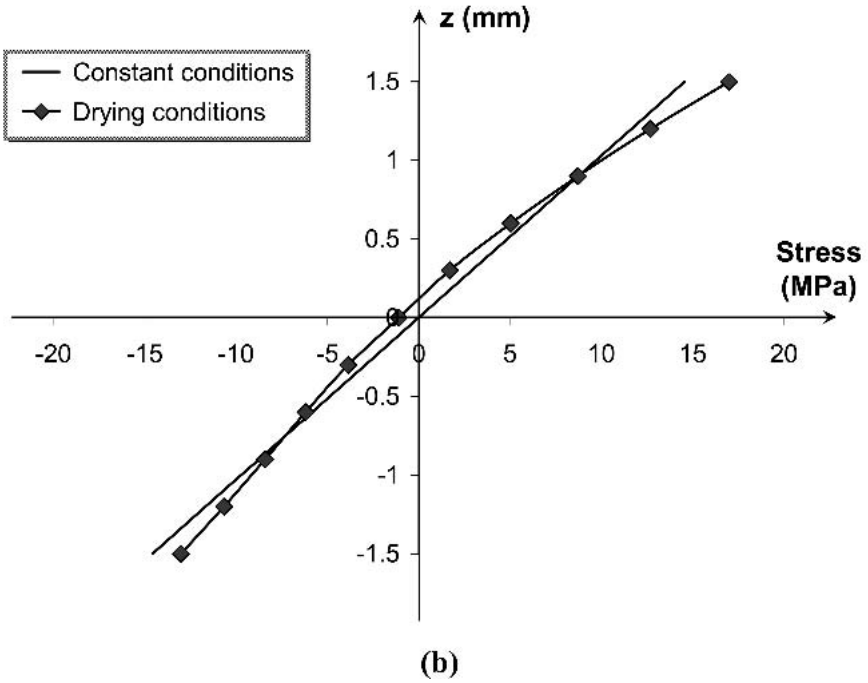

(b)

FIG. 8. Computed stress at $x = l/4$ under constant moisture conditions (18% MC and 30% SL); and under drying conditions (drying from 38% to 10% MC and 50% SL). a. Surface stress with time; b. Stress profile through thickness after 2 h of drying.

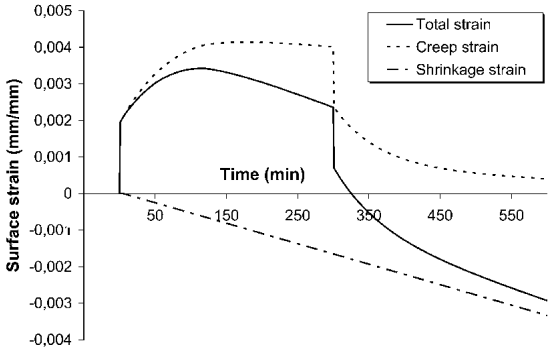

FIG. 9. Computed tensile surface strain in drying conditions (drying from 38% to 10% MC) for a 300-min loading (557 g) and unloading time.

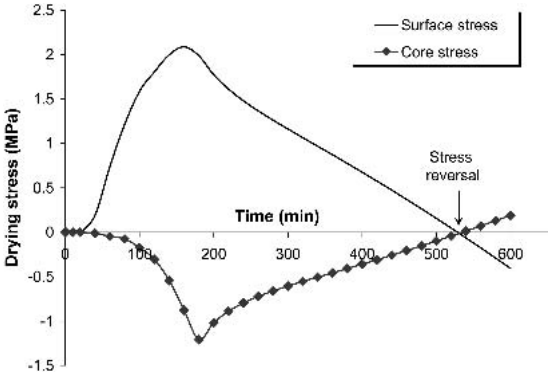

FIG. 10. Development of stress in the surface and center layers of the board during drying (from 35% to 10% MC).

face attempts to shrink but is restrained by the interior of the beam which is still above FSP. This constraint state of deformation induces tensile stresses within the surface layers and compressive stresses in the center of the cantilever.

The maximum tensile stress at the surface of the beam is approximately 2.1 MPa. This stress level is reached after 2.5 h of drying. The maximum compressive stress at the center in the same cross-section is approximately 1.2 MPa, and this after 3 h of drying. Stress reversal caused by the tension set at the surface appears after approximately 9 h of drying. These results are in good agreement with the experimental data reported in the literature (McMillen 1955; Cech 1964). Stress reversal takes place at too low moisture content, but this would be in great part due to the inaccuracy of the parameter values used for the rheological model.

CONCLUSIONS

The objective of this study was to develop a new approach of modeling the creep behavior of wood in a cantilever loaded at free end in relation to wood drying. The following conclusions can be drawn from this work:

- Using a rheological model and the proposed approach for the cantilever beam behavior under load, it is possible to estimate the strain and stress profiles at any position along the cantilever span without any assumption on the stress distribution through the thickness.
- The main advantage of the proposed approach is that it can be used to simulate experimental creep bending tests in the presence of moisture content gradients, and thus the nonlinear stress distribution. This allows the estimation of the parameters of any adopted rheological model using an optimization technique that minimizes the difference between experimental data (surface strain or deflection measurements) and numerical predictions.
- The cantilever technique allows simultaneous creep measurements in tension and in compression through surface strain measurements.
- Under no load conditions, the proposed modeling approach for the cantilever becomes a simple drying stress simulation model, which can predict drying stresses development in wood throughout the process.

Work is ongoing to test a more complete rheological model for the cantilever subjected to various moisture conditions.

ACKNOWLEDGMENTS

The authors are grateful for the financial support of this research from Natural Sciences and Engineering Research Council of Canada (No. 224297) and Forintek Canada Corp.

REFERENCES

BATOZ, J. L., AND G. DHATT. 1990. Modélisation des structures par éléments finis. Volume 2: Poutres et plaques. Hermès Éditions, Les Presses de l'Université Laval, Québec. 483 pp.

BENGTSSON, C. 1999. Mechano-sorptive creep in wood – experimental studies of the influence of material properties. Ph.D. Thesis, Department of Structural Engineering, Göteborg, Sweden.

BODIG, J., AND B. A. JAYNE. 1982. Mechanics of wood and wood composites, Van Nostrand Reinhold Co., New York, NY. 712 pp.

CASTERA, P. 1989. Tensile creep of small wood specimens across the grain under drying conditions. Pages 45–58 *in* Proc. 2nd International IUFRO Wood Drying Conference, Seattle, WA.

CECH, M. Y. 1964. Development of drying stresses during high-temperature kiln drying. Forest Prod. J. 14(2):69–76.

DAHLBLOM, O., H. PETERSSON, AND S. OMARSSON. 2001. Full 3-D FEM-simulations of drying distortions in spruce boards based on experimental studies. Pages 246–251 *in* Proc. 7th International IUFRO Wood Drying Conference, Tsukuba, Japan.

FRIDLEY, K. J., R. C. TANG, AND L. A. SOLTIS. 1992. Creep behavior model for structural lumber. ASCE J. Struct. Eng. 118(8):2261–2277.

GUITARD, D. 1987. Mécanique du matériau bois et composites. Éditions CEPADUES, Toulouse, France. 238 pp.

HANHIJÄRVI, A. 1999. Deformation properties of Finnish spruce and pine wood in tangential and radial directions in association to high temperature drying. Part II. Experimental results under constant conditions (viscoelastic creep). Holz Roh-Werkst. 57:365–372.

———, 2000. Deformation properties of Finnish spruce and pine wood in tangential and radial directions in association to high temperature drying: Part III. Experimental results under drying conditions (mechano-sorptive creep). Holz Roh-Werkst. 58:63–71.

HAQUE, M. N., T. A. G. LANGRISH, L.-B. KEEP, AND R. B. KEEY. 2000. Model fitting for visco-elastic creep of *Pinus radiata* during kiln drying. Wood Sci. Technol. 34:447–457.

HISADA, T. 1979. Creep and set behaviour of wood related to kiln drying. II. Effect of stress level on tensile creep of wood during drying. Mokuzai Gakkaishi 25:697–706.

———, 1980. Creep and set behaviour of wood related to kiln drying. IV. Effect of stress level on compressive creep and set of wood during drying. Mokuzai Gakkaishi 26:519–526.

———, 1986. Creep and set behavior of wood related to kiln drying. Forestry and Forest Products Research Institute. Report No. 335. Ibaraki, Japan. Pp. 31–130. (In Japanese)

HOYLE, R. J. JR., R. Y. ITANI, AND J. J. ECKARD. 1986. Creep of Douglas-fir beams due to cyclic humidity fluctuations. Wood Fiber Sci. 18(3):468–477.

HUNT, D. G. 1997. Dimensional change and creep of spruce, and consequent model requirements. Wood Sci. Technol. 31:3–16.

MÅRTENSSON, A. 1988. Tensile behavior of hardboard under combined mechanical and moisture loading. Wood Sci. Technol. 22:129–142.

———, AND S. SVENSSON. 1997. Stress-strain relationship of drying wood. Part I: Development of a constitutive model. Holzforschung 51:472–478.

MCMILLEN, J. M. 1955. Drying stresses in red oak: Effect of temperature. Forest Prod. J. 5(1):71–76.

MORÉN, T., S. MARGOT, AND B. SEHLSTEDT-PERSSON. 1993. Creep response to drying of timber boards of Scots pine. Forest Prod. J. 43(10): 58–64.

MOUTEE, M., A. LAGHDIR, M. FAFARD, AND Y. FORTIN. 2002. A three-dimensional mathematical model of the hygro-thermo-mechanical behavior of wood during drying. Pages 179–184 *in* Proc. Quality Drying: The Key to Profitable Manufacturing, Forest Product Society Conference, Montreal, Qc, Canada.

MUSZYŃSKI, L., R. LAGANA, AND S. M. SHALER. 2003. An optical method for characterization of basic hygro-mechanical properties of solid wood in tension. Pages 230–237 *in* Proc. 8th International IUFRO Wood Drying Conference, Brasov, Romania.

ORMARSSON S., O. DAHLBLOM, AND H. PETERSSON. 1999. A numerical study of the shape stability of sawn timber subjected to moisture variation. Part 2: Simulation of drying board. Wood Sci. Technol. 33:407–423.

PANG, S. 2001. Modelling of stresses and deformation of radiata pine lumber during drying. Pages 238–245 *in* Proc. 7th International IUFRO Wood Drying Conference, Tsukuba, Japan.

PASSARD, J., AND P. PERRÉ. 2001. Creep tests under water-saturated conditions: Do the anisotropy ratios of wood change with the temperature and time dependency? Pages 230–237 *in* Proc. 7th International IUFRO Wood Drying Conference, Tsukuba, Japan.

PERRÉ, P. 1996. The numerical modeling of physical and mechanical phenomena involved in wood drying: An excellent tool for assisting with the study of new processes. Pages 11–18 *in* Proc. 5th International IUFRO Wood Drying Conference, Québec, Canada.

RANTA-MAUNUS, A. 1975. The viscoelasticity of wood at varying moisture content. Wood Sci. Technol. 9:189–205.

———, 1992. Determination of drying stress in wood when shrinkage is prevented: Test method and modeling. Pages 139–144 *in* Proc. 3rd International IUFRO Wood Drying Conference, Vienna, Austria.

———, 1993. Rheological behaviour of wood in directions perpendicular to the grain. Mater. Struct. 26:362–369.

RICE, R. W., AND R. L. YOUNGS. 1990. The mechanism and development of creep during drying of red oak. Holz Roh-Werkst. 48:73–79.

SALIN, J. G. 1992. Numerical prediction of checking during timber drying a new mechano-sorptive creep model. Holz Roh-Werkst. 50:195–200.

SENFT, J. F., AND S. K. SUDDARTH. 1970. An analysis of creep-inducing stress in Sitka spruce. Wood Fiber Sci. 2(4):321–327.

SIMPSON, W. T. 1991. Dry kiln operator's manual. Agriculture Handbook No. 188, USDA Forest Products Laboratory, Madison, WI.

SVENSSON, S. 1995. Strain and shrinkage force in wood under kiln drying conditions. I: Measuring strain and shrinkage under controlled climate conditions. Equipment and preliminary results. Holzforschung 49(4):363–368.

———, 1996. Strain and shrinkage force in wood under kiln drying conditions. II: Strain, shrinkage and stress measurements under controlled climate conditions. Equipment and preliminary results. Holzforschung 50(5):463–469.

———, AND T. TORATTI. 2002. Mechanical response of wood perpendicular to grain when subjected to changes of humidity. Wood Sci. Technol. 36:145–156.

WU, Q., AND M. R. MILOTA. 1995. Rheological behavior of Douglas-fir perpendicular to the grain at elevated temperature. Wood Fiber Sci. 27(3):285–295.